



**HAL**  
open science

## Do transient hydrological processes explain the variability of strontium-90 activity in groundwater downstream of a radioactive trench near Chernobyl?

Mathieu Le Coz, Léa Pannecoucke, Albane Saintenoy, Chantal de Fouquet, Xavier Freulon, Charlotte Cazala

### ► To cite this version:

Mathieu Le Coz, Léa Pannecoucke, Albane Saintenoy, Chantal de Fouquet, Xavier Freulon, et al.. Do transient hydrological processes explain the variability of strontium-90 activity in groundwater downstream of a radioactive trench near Chernobyl?. *Journal of Environmental Radioactivity*, 2023, 259-260, pp.107101. 10.1016/j.jenvrad.2022.107101 . irsn-03951276

**HAL Id: irsn-03951276**

**<https://irsn.hal.science/irsn-03951276>**

Submitted on 23 Jan 2023

**HAL** is a multi-disciplinary open access archive for the deposit and dissemination of scientific research documents, whether they are published or not. The documents may come from teaching and research institutions in France or abroad, or from public or private research centers.

L'archive ouverte pluridisciplinaire **HAL**, est destinée au dépôt et à la diffusion de documents scientifiques de niveau recherche, publiés ou non, émanant des établissements d'enseignement et de recherche français ou étrangers, des laboratoires publics ou privés.



Distributed under a Creative Commons Attribution - NonCommercial - NoDerivatives 4.0 International License

# Do transient hydrological processes explain the variability of strontium-90 activity in groundwater downstream of a radioactive trench near Chernobyl?

Mathieu LE COZ<sup>1</sup>, Léa PANNECOUCKE<sup>1,2</sup>, Albane SAINTENOY<sup>3</sup>, Chantal de FOUQUET<sup>2</sup>, Xavier FREULON<sup>2</sup>, Charlotte CAZALA<sup>1</sup>

<sup>1</sup>Institut de Radioprotection et de Sûreté Nucléaire (IRSN), PSE-ENV/SEDRE, 92260 Fontenay-aux-Roses, France

<sup>2</sup>MINES ParisTech, PSL University, Centre for geosciences and geoengineering, 77300 Fontainebleau, France

<sup>3</sup>Université Paris-Saclay, CNRS, GEOPS, 91405, Orsay, France

## Abstract

The Chernobyl Pilot Site (CPS) was created in 2000 in order to study radionuclide migration processes to the geosphere from radioactive material of the Red forest buried in a trench. In this article, the data collected in the CPS up to 2015 are analyzed to identify the links between hydrological conditions and release of strontium-90 (<sup>90</sup>Sr) from the trench. Then, a flow-and-transport model is used for simulating distribution of <sup>90</sup>Sr both in the unsaturated and saturated zones downstream of the trench. The results show that the <sup>90</sup>Sr activity in groundwater is strongly transient in time, due to the high inter-annual variability of both the recharge rate and the groundwater level (some particularly wet winters resulted in saturation of the bottom part of the trench). In addition, the parameters that govern the sorption of <sup>90</sup>Sr in trench material appear to vary significantly in space (the retardation factor ranges from 10 to 50 depending on the location). This spatiotemporal variability could hide some critical processes, e.g., related to a long-term trend, and needs to be characterized through an appropriate sampling frequency.

**Keywords:** weather time-series; groundwater fluctuation; radioactive waste; groundwater modelling; variably saturated flow.

## 1. Introduction

### 1. Introduction

The Chernobyl accident of April 26, 1986 released large amounts of radionuclides which were deposited onto surrounding environment. In 1986 and 1987, emergency clean-up was undertaken in the Red Forest, an irradiated pine forest area, in the vicinity of the Chernobyl nuclear power plant, (Dzhepo et al., 1994). About  $500 \times 10^3$  m<sup>3</sup> of contaminated topsoil, vegetation and other radioactive materials were buried *in situ* in hundreds of trenches dug within the permeable sandy superficial formation, directly above groundwater table and without engineered moisture proof barriers (Kashparov et al., 2012). Cleared land was covered with 30 to 50 cm of sand to provide shielding from buried radioactive materials. Then, in 1988 and 1989, pine and birch trees were planted over the waste dump territory to limit erosion process.

Radionuclide migration from trenches to the geosphere remains a major concern, especially <sup>90</sup>Sr (strontium-90) due to its high mobility in soils and groundwater systems with respect to radiocesium and plutonium (Corcho-Alvarado et al., 2016) and to its possible incorporation by plants through calcium and potassium transporters (Burger and Lichtscheidl, 2019). Investigation of radionuclide migration processes, including field characterization and development of theoretical models, was one of the main issues tackled as part of the cooperation between French and Ukrainian research teams between 1998 and 2017, through a multidisciplinary program deployed on the Chernobyl Pilot Site

(Dewiere et al., 2004). This experimental facility developed around the trench n°22 (T22) is comparable to other sites with surface burial of radioactive waste, e.g., Hanford Site (Steeffel et al., 2003; Zhuang et al., 2007) or White Oak Creek (McCarthy et al., 1998; Garten, 1999). However, a relatively simple geological situation contributes to a more thorough separation of hydraulic from geochemical phenomena (Van Meir et al., 2009).

The trench T22 has been largely monitored, allowing an advanced characterization of site geology, water flow regime in unsaturated and saturated zones, radionuclide distribution and speciation within and outside the trench (e.g., Bugai et al., 2012a; Kashparov et al., 2012; Le Gal La Salle et al., 2012; Van Meir et al., 2012). Then, data and knowledge acquired were integrated into numerical flow-and-transport models to simulate transfer of  $^{90}\text{Sr}$  from the trench to the underlying aquifer (Bugai et al., 2012a; Nguyen, 2017). However, these models did not satisfactorily reproduce  $^{90}\text{Sr}$  activity measured on wells located downstream of the trench. Model weaknesses presumably came from a limited conceptual framework, with a misrepresentation of temporal variability both of hydrological and geochemical conditions (Bugai et al., 2012a).

Indeed, uncoupled unsaturated and saturated flow processes were considered. Survey of water table level yet highlighted that it rose above the T22 trench bottom elevation several times between 2000 and 2015 (Nguyen, 2017). Saturation of the lower part of waste repository could have increased diffusive exchange between porewater and mobile water (Fretwell et al., 2005) and resulted in major radionuclide (especially  $^{90}\text{Sr}$ ) release events to groundwater (Bugai et al., 2012b). In addition, the total inventory of  $^{90}\text{Sr}$  was used as model source term rather than the ion-exchangeable  $^{90}\text{Sr}$ . This could have resulted in a significant overestimation of the simulated  $^{90}\text{Sr}$  activity in groundwater (Nguyen, 2017) since the  $^{90}\text{Sr}$  was initially embedded in fuel particles and was not available for transport with mobile water (Dewiere et al., 2004; Kashparov et al., 2012).

The aim of this paper is to reinforce the model of migration of  $^{90}\text{Sr}$  from the trench T22 to groundwater, based on a better representation of the transient processes. First, data and knowledge about variability in hydrological conditions, namely weather and water level, and about kinetic of release of ion-exchangeable  $^{90}\text{Sr}$  from the waste are summarized and analyzed regarding the available  $^{90}\text{Sr}$  activity measurements (see Section 3). Then, the resulting updated parameters and boundary conditions are implemented in a flow-and-transport model with a modified conceptual framework (see Section 4). Finally, the links between temporal variability of hydro-geochemical conditions and release of  $^{90}\text{Sr}$  to groundwater are discussed. This analysis provides a more comprehensive view of the data survey to implement for characterizing the mobility of radionuclides from *in situ* waste disposals (see Section 5).

## **2. The Chernobyl Pilot Site (CPS)**

### 2.1. Overview

The Chernobyl exclusion zone covers about 30 km around the Chernobyl Nuclear Power Plant. It is situated on a Quaternary glacial plateau with a mostly flat surface and incised by the Prypiat River hydrographic network. Dominant land cover types are woodlands and marshlands while major urban centers, cities of Chernobyl and Pripjat, are uninhabited since 1986. Land abandonment has led to an expansion of dense and sparse forest areas at the expense of grassland areas (Gemitzi, 2020).

The Chernobyl Pilot Site (CPS) is located 2.5 km south west of the Nuclear Power Plant, in central part of the first terrace of Pripjat River (Fig. 1b). The area is part of the Red forest, where acute irradiation due to initial radioactive deposits caused the death of Scots pine trees over more than 1,500 ha (Thiry et al., 2009). After the accident, radioactive materials, including contaminated trees, topsoil layer and forest litter were buried in trenches, and the area was planted with a combination of pine and birch

trees as well as bushes to prevent secondary contamination due to soil erosion or wind resuspension (Kashparov et al., 2012).

## 2.2. Geological settings

The Chernobyl exclusion zone mainly extends over the northwestern slope of the Ukrainian Shield. Crystalline basement is covered with 130 to 190 m of Mesozoic and Cenozoic sedimentary deposits (Matoshko et al., 2004). Exposed member consists of about 30 m of Upper Pleistocene - Holocene sand, subdivided into alluvial and eolian suites, which overlays dense marine carbonate silts and marls of the Kiev Suite of Eocene.

Grain-size distribution analysis of material cored in the CPS allowed identification of different genetic types of deposits within the Upper Pleistocene - Holocene formation (Bugai et al., 2012a), from the top to the bottom: (i) 0.5 to 0.8 m of contemporary forest podzols or soil displaced during clean-up operations; (ii) about 4 m of eolian deposits (well sorted fine-medium grained sand with clay content lower than 1%); (iii) about 4 m of alluvial deposits of floodplain facies (sand with clay content up to 8%) or dead-channel facies (loamy-clayey sand); and (iv) about 20 m of alluvial deposits of channel facies (well-sorted medium-grained sand with a low clay content).

## 2.3. General subsurface hydrogeology

The Upper Pleistocene - Holocene deposits host an unconfined aquifer, lying on a regional aquitard layer composed of marls of the Kiev suite (Matoshko et al., 2004). Thickness of unsaturated zone varies from 0 to 10 m. Flat relief with predominance of sandy deposits in the upper part of soil section favours high rates of meteoric water infiltration to groundwater system (Bugai and Dewiere, 2004). Regional flow is directed to the Pripjat River and amplitude of seasonal fluctuations of water table level is 0.5 m to 2 m depending on area.

In the CPS area, groundwater table generally varies from 3 to 4 m deep and groundwater flows towards the Pripjat River (Bugai et al., 2012a). It should be noted that wetlands with temporary surface water storage are present west of the CPS and may have seasonal influence on groundwater flow regime locally (Bugai and Dewiere, 2004).

## 2.4. The Chernobyl Pilot Site (CPS) and the trench T22

The CPS covers an area of roughly 100 × 100 m around the trench T22 (Fig. 1c), with a mean ground surface elevation of 115 m above sea level. Boreholes and ground-penetrating radar surveys (Saintenoy et al., 2017) allowed to identify the geometry of the trench, i.e., about 70 m long, 6 m wide and 3 m deep. External gamma radiation exposure dose rate 1 m above ground surface is of  $\times 10 \mu\text{Gy}\cdot\text{h}^{-1}$  (Kashparov et al., 2012) and average specific activities of  $^{90}\text{Sr}$  and  $^{137}\text{Cs}$  (cesium-137) in the trench are about  $10^5$  to  $10^6 \text{ Bq}\cdot\text{kg}^{-1}$  (Dewiere et al., 2004; Van Meir et al., 2009). The CPS has been instrumented since 2000 for surveying meteorological parameters (weather station), buried material (boreholes), underlying unsaturated zone (soil water samplers) and saturated zone (wells) through either continuous monitoring or periodic sampling and analysis (Fig. 1c) (Kashparov et al., 2012).

## **3. Data analysis**

In this Section, weather and water level time series recorded at the CPS are completed over the whole 1987-2020 period based on a climate database and a lumped conceptual model. In addition, results of two previous works, which focused on (i) the initial inventory of  $^{90}\text{Sr}$  embedded in fuel particles in the trench T22 and (ii) the dissolution of these fuel particles, are combined for estimating the release of

$^{90}\text{Sr}$  in ion-exchangeable form in time since 1987. Finally, activities of  $^{90}\text{Sr}$  measured in groundwater downstream from the trench T22 are depicted.

### 3.1. Data and models

#### *3.1.1. Weather*

Weather parameters (precipitation, air/soil temperature, wind speed, solar radiation) were recorded on the CPS with 1-hour time step from 2000 to 2011 (Fig. 1c). These parameters are used for estimating potential evapotranspiration (PET) based on hourly FAO Penman-Monteith equation (Allen et al., 1998). Precipitation, air temperature and PET are then aggregated at a daily time step.

Daily precipitation computed for the CPS is compared with daily precipitation at four rain gauges located within a 100 km radius from Chernobyl and released by the European Climate Assessment & Dataset (ECA&D) project (Klein Tank et al., 2002). Data from the CPS are consistent with data collected at Bragin (40 km north from Chernobyl, Fig. 1a) (Table 1), especially regarding cumulative precipitation and number of wet days (i.e., days with precipitation > 0.5 mm). The time series of daily precipitation for the CPS is extended from 1987 to 2020 by using precipitation data from Bragin.

Daily temperature (minimum, maximum and average) recorded at a weather station in Kiev (100 km south from Chernobyl, Fig. 1a), and also released by the ECA&D project, are used for estimating daily PET based on Hargreaves equation (Hargreaves and Allen, 2003). Based on linear regressions, it appears that daily average temperature in Kiev is 0.8° higher than temperature at the CPS; and daily PET in Kiev is 24% higher than PET estimated for the CPS but these highly correlated (Pearson correlation coefficient > 0.9). Average temperature and PET time series computed for the CPS from 2001 to 2011 are extended on the 1987-2020 period by reducing of 0.8°C and 24% respectively the observation data from Kiev.

#### *3.1.2. Water table level and percolation*

Water table level was recorded with 6-hours time step from 2000 to 2015 through automatic probes installed in five wells screened from 109.5 m to 110.5 m (Fig. 1c). Manual measurements were performed monthly in those wells and are used for calibrating automatic probe data. Data are then aggregated at a daily time step. Only the time series computed at one well (well 2-99) is complete for the whole 2000-2015 period (records ended in 2010 for the other wells).

To extend this time series from 1987 to 2020, a lumped conceptual model is built. It simulates percolation through the unsaturated zone, and groundwater level fluctuations based on precipitation, temperature and PET. This model reproduces water cycle processes through successive reservoirs representing snowpack, soil, unsaturated and saturated zones (Annex 1). Model parameters are first calibrated to simulate variations in water table level consistent with the monitored time series at the well 2-99 for the 2000-2015 period; then, the calibrated parameters are used on the whole 1987-2020 period.

#### *3.1.3. Total and ion-exchangeable $^{90}\text{Sr}$*

In 1999, 2002, 2003 and 2015, about 200 boreholes were drilled up to 3 m deep on a mesh through the trench T22 and the underlying unsaturated sand (Fig. 1c), and *in situ* measurements of gamma-emission profiles were performed using a submersible counting probe (Bugai et al., 2002). In 1999, about 100 samples of material were collected from these boreholes for radionuclide activity measurements, especially  $^{137}\text{Cs}$ ,  $^{90}\text{Sr}$  and  $^{154}\text{Eu}$  (europium-154), through alpha-, beta- and gamma-

spectrometry (with radiochemical extraction of  $^{90}\text{Sr}$  and transuranic radionuclides) (Kashparov et al., 2004, 2012).

Specific activity of  $^{137}\text{Cs}$  was estimated for each gamma-emission profile based on an empirical correlation between gamma-count rate and radionuclide content measured on the collected samples (Bugai et al., 2002). A geostatistical analysis of resulting individual activity values were used for simulating in three dimensions (3-D) the spatial distribution of  $^{137}\text{Cs}$  activity in the trench in 2000 (Bugai and Dewiere, 2003; Bugai et al., 2005; Nguyen, 2017). Activity of  $^{137}\text{Cs}$  in 2000 is converted in initial (i.e., in 1987) activity of total  $^{90}\text{Sr}$  by considering empirical  $^{137}\text{Cs}$ - $^{154}\text{Eu}$  ratio in 2000 and  $^{154}\text{Eu}$ - $^{90}\text{Sr}$  ratio in Chernobyl reactor fuel particles (Annex 2).

Strontium-90 in Chernobyl fallout were embedded in micron-sized particles of dispersed nuclear fuel. Observations during post-accident phase showed that these fuel particles are subject to gradual dissolution that results in release of  $^{90}\text{Sr}$  in ion-exchangeable form, i.e.,  $^{90}\text{Sr}$  mobilizable by percolation water (Dewiere et al., 2004; Kashparov et al., 2012). Based on laboratory experiments on waste material from the trench T22, a dissolution model was built for estimating this release since 1987 from the initial activity of total  $^{90}\text{Sr}$  established (Annex 2).

#### *3.1.4. Migration of $^{90}\text{Sr}$ in groundwater*

From 2000 to 2015, activity of  $^{90}\text{Sr}$  in groundwater collected in the well network surrounding the trench T22 (Fig. 1c) was measured by liquid scintillation counting. Wells are screened at four sampling levels: 110.5-111.5 m (level 1, L1); 109.5-110.5 m (L2); 107.5-109.5 m (L3); and 105.5-107.5 m (L4). Sampling was performed generally once or twice a year into two series of wells aligned orthogonally to the trench and assumed to be parallel to groundwater flow lines, the so-called A-B (24 sampling points, eastern part of the trench) and C-D (14 sampling points, center-western part of the trench) cross-sections (Fig. 1c).

### 3.2. Time series

#### *3.2.1. Weather*

Mean annual precipitation for the 1960-2020 period is 540 mm, with a monthly maximum in July (75 mm) and a monthly minimum in February (25 mm) (Fig. 2a). Mean annual PET and average temperature are 550 mm and 7°C, with monthly values higher than 80 mm and 14°C from May to August and lower than 10 mm and 0°C from November to February (Figs. 2b/c). Mean monthly precipitation is higher than mean monthly PET from October to March (called winter months hereafter).

Since 1987, annual precipitation does not show any evident trend. The maximum cumulative amounts (> 700 mm) occurred in 1999, 2011 and 2013; the minimum (< 400 mm) in 2015, 2019 and 2020. (Fig. 2d). Precipitation during the winter period shows marked peaks (> 300 mm) in 2004, 2011, 2013 and 2017. Since 1998, annual PET is higher than the average 1959-2020 value (except in 2004) (Fig. 2e), in relation with an increasing trend in mean summer temperature (+ 0.08°C per year since 1987) (Fig. 2f).

#### *3.2.2. Water table level and percolation*

During the 2000-2015 period, water table level varied from 110.7 m in October 2003 to 112.8 m in April 2013 (Fig. 3a). Intra-annual range was generally about 0.7 m from October (minimum) to April (maximum). Some recharge events yet resulted in more marked increases (> 1m), especially in 2004, 2011 and 2013. Except during these years, water table level appears to follow an inter-annual

decreasing trend. Simulated time series well reproduces inter-annual variability during the 2000-2015 period but appears to smooth some high-frequency variations (Fig. 3b; Annex 1).

Based on the calibrated groundwater level fluctuation model, maximum water table level in 1987 is estimated to be 111.5 m, and it then remains below this value until 1999 (Fig. 3b). Since 2015, a peak is simulated in 2017-18, between two drop periods. In addition, yearly cumulative percolation appears to be linked to precipitation amount, especially during the winter periods (Pearson Correlation Coefficient > 0.8) (Table 2). Percolation corresponds to about 40% ( $\pm 10\%$  depending on the year) of yearly precipitation.

### 3.2.3. Total and ion-exchangeable $^{90}\text{Sr}$

Based on the 3-D simulation of  $^{137}\text{Cs}$  inventory in 2000 established by Nguyen (2017) (Annex 2), the initial inventory of total  $^{90}\text{Sr}$  in the trench T22 is estimated to be  $330 \pm 6$  GBq (Fig. 4a). More specifically, the mean inventories related to the cross-sections A-B (Fig. 4b) and C-D (Fig. 4c) are estimated to be 6.9 and 10.3 GBq. Based on the dissolution model of fuel particles, the cumulative activity of  $^{90}\text{Sr}$  in ion-exchangeable form (still in the trench or having migrated in the surrounding environment) has been stabilized to about 25% of the initial inventory of total  $^{90}\text{Sr}$  since 2000, the dissolution rate being counterbalanced by the radioactive decay (Fig. 5).

The migration of  $^{137}\text{Cs}$  and  $^{90}\text{Sr}$  in the unsaturated sand is analyzed for the boreholes b12/311 and b21/303 (Figs. 4a), where the trench thickness is relatively thin, of about 1 m. The mean activity in  $^{137}\text{Cs}$  in the trench in 2000 is of  $2 \times 10^5$  Bq.kg $^{-1}$  (Fig. 6a/b). Below the trench,  $^{137}\text{Cs}$  activity drops abruptly to less than  $1 \times 10^3$  Bq.kg $^{-1}$ . The measured activity of total  $^{90}\text{Sr}$  in 2000 in waste is higher than  $5 \times 10^4$  Bq.kg $^{-1}$ , and then decreases progressively below the trench. This decrease is more marked in the borehole b12/311 ( $1 \times 10^4$  Bq.kg $^{-1}$  at 112.5 m, Fig 6a) than in the borehole b21/303 ( $1 \times 10^3$  Bq.kg $^{-1}$  at 112.5 m, Fig 6b). In addition, the measured activity of total  $^{90}\text{Sr}$  in 2000 in waste is generally lower than theoretical activity estimated from  $^{137}\text{Cs}$  inventory (estimation that does not consider migration from 1987 to 2000) and higher than theoretical activity of  $^{90}\text{Sr}$  in ion-exchangeable form estimated from  $^{137}\text{Cs}$  inventory and dissolution model.

### 3.2.4. Migration of $^{90}\text{Sr}$ in groundwater

Distribution of activity of  $^{90}\text{Sr}$  measured during the 2000-2015 period in the wells of the cross-section A-B, i.e., six locations separated of about 5 m each (AP1 to AP6, from upstream to downstream of the trench T22) with four sampling depths (layers L1 to L4, from top to bottom), shows that (Fig. 7a-d):

- i. Along the top layer (L1), mean  $^{90}\text{Sr}$  activity progressively increases below the trench (from 100 to 3,000 Bq.l $^{-1}$ , from AP1 to AP4).
- ii. Along the layers L2 and L3, peaks of activity respectively occur in AP4 and AP5 (1,000 Bq.l $^{-1}$ ) and in AP5 (800 Bq.l $^{-1}$ ).
- iii. Mean activity decreases from AP5 to AP6 for the layers L1 to L3, whereas there is no significant change observed along the layer L4.

Distribution of activity of  $^{90}\text{Sr}$  activity measured during the 2000-2015 in the wells of the cross-section C-D, i.e., three locations (CP2 to CP4, from upstream to downstream) with four sampling depths (layers L1 to L4, from top to bottom) and two locations with one sampling depth (CP1-L2 and CP5-L2), shows a spatial dynamic comparable with evolution described along the cross-section A-B (Fig. 7e-h). However, measured activities are significantly higher, of about one order of magnitude, for layers L1 to L3 (except in the well CP2-L2).

The sampling frequency is too low for characterizing the temporal variability of  $^{90}\text{Sr}$  activity. Nevertheless, several observations can be made along the two cross-sections A-B and C-D (Fig. 8), especially:

- i. In AP4-L1 (geometric mean of measured activities of 2,500 Bq.l<sup>-1</sup>) and CP2-L1 (geometric mean of 25,000 Bq.l<sup>-1</sup>), a very significant peak of activity (over 10,000 Bq.l<sup>-1</sup> / 60,000 Bq.l<sup>-1</sup>) occurred in May 2005 and less marked peaks (7,000 Bq.l<sup>-1</sup> / 30,000 Bq.l<sup>-1</sup>) occurred in 2001 (at least in AP4-L1) and 2009.
- ii. In AP5-L2 (geometric mean of 1,000 Bq.l<sup>-1</sup>) and CP3-L2 (geometric mean of 7,000 Bq.l<sup>-1</sup>), high activity values or increasing trend are noticed before 2007 (up to 2,000 / 25,000 Bq.l<sup>-1</sup>) and a decreasing trend appears to occur then.
- iii. In AP6-L2 (geometric mean of 400 Bq.l<sup>-1</sup>) and CP5-L2 (geometric mean of 3,500 Bq.l<sup>-1</sup>), relatively low activity values were measured until 2003 (200 / 2,000 Bq.l<sup>-1</sup>). Then, activity values are scattered close to the mean, and higher values are noticed after 2013 (1,200 / 7,000 Bq.l<sup>-1</sup>).

#### 4. Flow-and-transport modelling

In this Section, a physically-based flow-and-transport model is built for reproducing the migration of the  $^{90}\text{Sr}$  released from the trench T22 to the underlying unsaturated sand in the boreholes b12/311 and b21/303, and then to the groundwater along the cross-sections A-B and C-D. The influence of the hydro-climatic variability on the  $^{90}\text{Sr}$  migration is assessed by modifying some model parameters and boundary conditions.

##### 4.1. Model setting

###### 4.1.1. Numerical code

The MELODIE numerical code (IRSN, 2009, Pannecoucke et al., 2019) solves in 2-D the generalized Richards equation (Eq. 1) describing flow in variably saturated porous media, and an advection-dispersion-reaction equation (Eq. 2) representing migration of radionuclides:

$$\frac{\partial \theta}{\partial t} + S_S S_w(\theta) \frac{\partial \psi}{\partial t} + \nabla \cdot (K(\psi) \nabla(\psi + z)) = q_{SS} \quad \text{Eq. 1}$$

where  $\theta$  is the volumetric moisture content [L<sup>3</sup>.L<sup>-3</sup>],  $t$  is the time [T],  $S_S$  is the specific storage [L<sup>-3</sup>],  $S_w$  is the water saturation [-],  $\psi$  is the water pressure head [L],  $K$  is the hydraulic conductivity tensor [L.T<sup>-1</sup>],  $z$  is the vertical coordinate directed upward [L], and  $q_{SS}$  is the distributed source (positive) or sink (negative) term [L<sup>3</sup>.L<sup>-3</sup>.T<sup>-1</sup>];

$$\nabla \cdot [(D|\vec{u}| + \omega d) \nabla C - \vec{u}C] = \omega' R \frac{\partial C}{\partial t} + \omega' \lambda RC \quad \text{Eq. 2}$$

where  $D$  is the dispersivity tensor [L],  $\vec{u}$  is the pore water velocity [L.T<sup>-1</sup>],  $\omega$  and  $\omega'$  are the total and the effective porosities [L<sup>3</sup>.L<sup>-3</sup>],  $d$  is the molecular diffusion coefficient [L<sup>2</sup>.T<sup>-1</sup>],  $C$  is the volumetric radionuclide concentration [M.L<sup>-3</sup>],  $R$  is the retardation factor [-], and  $\lambda$  is the radioactive decay constant [T<sup>-1</sup>]. It should be noted that radionuclide retention on soil is governed by the retardation factor ( $R$ ), based on the linear equilibrium sorption concept also called the  $K_d$  approach (Balonov et al., 2010),  $K_d$  [L<sup>3</sup>.M<sup>-1</sup>] being the exchangeable equilibrium coefficient such as:

$$R = \frac{\rho K_d}{\theta} \quad \text{Eq. 3}$$

where  $\rho$  is the soil bulk density [M.L<sup>-3</sup>].

Besides, MELODIE is coupled with the dissolution model of fuel particles (Annex 2), which allows to simulate at each time-step the release of  $^{90}\text{Sr}$  in ion-exchangeable form from the initial inventory of total  $^{90}\text{Sr}$ .

#### 4.1.2. Migration of $^{90}\text{Sr}$ in the unsaturated zone

Migration of  $^{90}\text{Sr}$  released from the trench to the underlying unsaturated sand is simulated from 1987 to 2000 at a daily time step by considering a 5 m height (discretized into 101 nodes)  $\times$  1 m wide vertical section (2 nodes). The daily percolation rate simulated with the calibrated groundwater fluctuation model (Annex 1) is used as upper boundary condition (time variable specified fluxes) and the simulated water table level as lower boundary condition (specified heads).

The flow-and-transport parameters are estimated based on previous analyses of data from unsaturated flow survey and tracer test experiments (Bugai et al., 2012a, Nguyen, 2017) (Table 3). Due to high uncertainty regarding the retardation factor ( $R$ ) that governs the linear equilibrium sorption of trench material, the model is run with various  $R$  values (Table 3). The source term consists of 1 m thick of total  $^{90}\text{Sr}$  with an activity of  $1.3 \times 10^5 \text{ Bq.kg}^{-1}$ , which corresponds to an activity of  $^{137}\text{Cs}$  in 2000 of  $2 \times 10^5 \text{ Bq.kg}^{-1}$  (Annex 2). The vertical profiles of  $^{90}\text{Sr}$  activity simulated in 2000 can thus be compared with the measured activities in the boreholes b12/311 and b21/303 (see section 3.2.3).

#### 4.1.3. Migration of $^{90}\text{Sr}$ in groundwater

Migration of  $^{90}\text{Sr}$  released from the sections A-B and C-D of the trench to the upper part of the aquifer, i.e., eolian sand and alluvial deposits of floodplain facies, is simulated from 1987 to 2015 at a daily time step by considering 2-D cross-sections with 10 m height (discretized in 76 nodes)  $\times$  80 m wide (81 nodes). Flow boundary conditions are defined as follows:

- i. Time variable hydraulic head corresponding to the daily water table elevation simulated with the calibrated groundwater fluctuation model (Annex 1) is set on the both sides of the domain; a horizontal hydraulic gradient of  $1.5 \times 10^{-3} \text{ m.m}^{-1}$  is considered.
- ii. No-flow condition is fixed on the bottom boundary; hydraulic conductivity of the bottom node layer is set so as to represent the lower part of the aquifer, i.e., about 20 m of alluvial deposits of channel facies.
- iii. Time variable flow corresponding to the daily percolation rate simulated with the calibrated groundwater fluctuation model (Annex 1) is imposed on the top boundary.

The flow-and-transport parameters are estimated based on previous work (Table 3). The source term consists of the mean initial inventory of total  $^{90}\text{Sr}$  related to the cross-sections A-B (Fig. 4b) or C-D (Fig. 4c) computed based on the 3-D simulation of the  $^{137}\text{Cs}$  inventory in 2000 established by Nguyen (2017). Simulated time series of  $^{90}\text{Sr}$  activity in the observation wells can thus be compared with the measured activities in groundwater samples from 2000 to 2015 (see section 3.2.4).

In addition, in order to assess the influence of hydro-climatic variability on migration of  $^{90}\text{Sr}$ , the model is run with the following modified boundary conditions:

- i. On the both sides of the domain, time variable hydraulic head is replaced by a constant value, namely the average of the in initial time series (111.5 m).
- ii. On the top boundary, time variable flow is replaced by a constant value, namely the average of the time series ( $0.57 \text{ mm.d}^{-1}$ ).

## 4.2. Results

#### 4.2.1. Migration of $^{90}\text{Sr}$ in the unsaturated zone

The model reproduces the progressive decrease of  $^{90}\text{Sr}$  activity in unsaturated sand below the trench as highlighted on measurements in 2000 (Fig. 9). The intensity of this decrease depends on the value set for the retardation factor ( $R$ ) of the waste material: the simulated vertical profile of  $^{90}\text{Sr}$  activity is consistent with the measurements in the borehole b21/303 with a  $R$  value of 10 ( $K_d=2 \text{ l.kg}^{-1}$ ); whereas the measurements in the borehole b12/311 are better reproduced with a  $R$  value of 25 ( $K_d=6 \text{ l.kg}^{-1}$ ).

The cumulative amount of  $^{90}\text{Sr}$  that had migrated from the trench to underlying sand is estimated to about 50% of the cumulative amount of  $^{90}\text{Sr}$  released in ion-exchangeable form into the trench when the  $R$  retardation factor is set to 10; and to about 20% of this amount with a  $R$  value of 25.

#### 4.2.2. Migration of $^{90}\text{Sr}$ in groundwater

The simulated  $^{90}\text{Sr}$  plumes spread in eolian sand (layers L1 and L2) up to the domain boundary (i.e., 40 m) downstream of the trench with a downward component (Fig. 10), in accordance with the measurements. Moreover, the simulated activity of  $^{90}\text{Sr}$  decreases abruptly at the interface between eolian sand and alluvial deposits of floodplain facies (layer L3), which is consistent with both low intensity and low variability of activities measured along the layer L4.

The simulated activity of  $^{90}\text{Sr}$  depends on the  $R$  value set for waste material: the orders of magnitude highlighted from the measurements appear to be reproduced with a  $R$  value of 50 ( $K_d=12 \text{ l.kg}^{-1}$ ) for the cross-section A-B (Fig. 11); and with a  $R$  value of 13 ( $K_d=3 \text{ l.kg}^{-1}$ ) for the cross-section C-D (Fig. 12). By considering these  $R$  values, simulated temporal variability of  $^{90}\text{Sr}$  activity in the observation wells is generally consistent with the measurements, although discrepancies appear for some of the wells (e.g., highest  $^{90}\text{Sr}$  activities measured in 2005 in the wells AP4-L1 and CP2-L1 are underestimated by the model). Overall, the simulated time series show an increasing trend of the activity of  $^{90}\text{Sr}$  from 1987 to 2015; and three main peaks of  $^{90}\text{Sr}$ , in 2001, 2005/2006 and 2013/2014, i.e., following the wettest periods. In addition, the cumulative amount of  $^{90}\text{Sr}$  that had migrated from the cross-sections A-B and C-D are estimated to correspond to about 50% and 67% of the cumulative amount of  $^{90}\text{Sr}$  released in ion-exchangeable, respectively.

When considering a constant groundwater level (Fig. 13), the temporal variability of the simulated time series of  $^{90}\text{Sr}$  activity is preserved along the top layer (L1). Along the layer 2, both the peak intensity and the increasing trend after 2000 are less marked, and the peaks appears to be delayed. When considering a constant recharge rate (Fig. 13), the times series along the layer L2 are preserved whereas along the layer L1, the peaks of activity are delayed. However, the boundary conditions do not affect significantly the cumulative amount of  $^{90}\text{Sr}$  that had migrated from the trench ( $\pm 1\%$ ).

## 5. Discussion

### 5.1. Hydro-climatic parameters

During the last two decades, cumulative precipitation during winter periods, i.e., from October to March, was the main driver of inter-annual variation of water table level in the CPS area. Hence, some particularly wet winters resulted in water table level higher than the level simulated in 1987 when the trench T22 was dug, thus in saturation of the bottom part of the trench. A first high water table level period was simulated in 1999 and the most significant ones (0.5 to 1 m above the trench bottom) occurred in 2004 and 2013. Saturation periods were longer for the trench cross-section C-D than for the cross-section A-B (49% and 18% of the days from 2000 to 2015, respectively) since the trench bottom is deeper along C-D. Groundwater survey shows that such high water table levels could have resulted in temporary increase in groundwater  $^{90}\text{Sr}$  activity in the upper part of the aquifer. However,

the sensitivity analysis performed based on the flow-and-transport model shows that these events did not impact significantly the inter-annual amount of  $^{90}\text{Sr}$  released in groundwater. Accordingly, when considering similar model configurations, especially the same  $R$  value for waste material, the simulated activity of  $^{90}\text{Sr}$  in groundwater downstream of the trench is comparable for both the cross-sections A-B and C-D despite a longer saturation of the bottom part of the trench along C-D.

High reactivity of water table fluctuation to precipitation involves a low soil water holding capacity (about 20 mm, according to the groundwater fluctuation model), which is consistent with the fact that the soil was partly removed during the clean-up operation. Yearly cumulative percolation simulated with the calibrated groundwater fluctuation model corresponds to about 40% ( $\pm 10\%$  depending on the year) of the precipitation amount. Simulated percolation is yet generally lower (up to 30%) than the recharge rate estimated on the CPS area using the water table fluctuation analysis method (WTF, Healy and Cook, 2002) from 2000 to 2012 (Saprykin et al., 2015) (Table 4). Several reasons could explain this difference: the WTF method was applied on each single recharge event whereas the calibrated model tends to smooth some intra-annual variations of water table level; and simulated percolation could represent a net flow, which integrates plant uptakes, including from the saturated zone. Nevertheless, the percolation rate simulated with the calibrated groundwater calibration model is a relevant input for the flow-and-transport model. Indeed, it allows to reproduce the order of magnitude of activity of  $^{90}\text{Sr}$  measured in both the unsaturated and the saturated zones. It should be noted that this model does not consider plant uptake so the percolation rate corresponds to a net flow; and over- or under-estimation of the percolation rate could be compensated through other model parameters such as the  $R$  retardation factor of the waste material.

Inter-annual increasing trend of potential evapotranspiration (PET), in relation with increase of average summer temperature (about  $+0.08^\circ\text{C}\cdot\text{yr}^{-1}$ ), does not appear to significantly impact actual uptakes from soil (this process is not considered by the flow-and-transport model). In a context of relative shallow water table (about 5 m deep), actual withdrawals due to plant transpiration could be more related to water table level than to potential demand (i.e., PET), since plant roots tap groundwater (Roebroek et al., 2020).

## 5.2. Migration of $^{90}\text{Sr}$

Soil activity profiles indicate that  $^{90}\text{Sr}$  in ion-exchangeable form produced from the trench waste had partly migrated downward into the unsaturated zone, up to 2 m deep from 1987 to 2000. The flow-and-transport model shows that this migration can be reproduced by considering reversible  $^{90}\text{Sr}$  sorption processes within both waste material and underlying sand, e.g., through the linear equilibrium sorption concept, combined with a vertical percolation flow. The reversibility of the  $^{90}\text{Sr}$  sorption in the Chernobyl eolian sandy deposit was already highlighted through laboratory experiments (Ardois and Szentnect, 2005). These experiments also showed that the  $^{90}\text{Sr}$  sorption can be perfectly described by the same ion exchange model whatever the water content. The flow-and-transport model applied on both the unsaturated profiles and the saturated cross-sections yet suggests that parameters that govern sorption in waste material vary significantly in space: the retardation factor ( $R$ ) could range from 10 ( $K_d=2 \text{ l}\cdot\text{kg}^{-1}$ ) to 50 ( $K_d=12 \text{ l}\cdot\text{kg}^{-1}$ ) depending on the location. Such a range involves high spatial variability in the amount of  $^{90}\text{Sr}$  released, which needs to be taken into consideration for establishing a budget at the trench scale.

Survey of  $^{90}\text{Sr}$  activity into groundwater clearly shows a contamination downstream of the trench T22. Measured  $^{90}\text{Sr}$  activity values are highly variable in time and remain difficult to interpret since sampling frequency is shorter than frequency related to the main processes that govern release of radionuclides into groundwater. Nevertheless, the flow-and-transport model results in time series of  $^{90}\text{Sr}$  activity

consistent with most of the measurements: temporal variability of measured  $^{90}\text{Sr}$  activity can thus be linked, at least in part, to inter-annual variability of both the recharge rate and the groundwater level. The flow-and-transport model yet does not reproduce intensity of the highest peaks of  $^{90}\text{Sr}$  activity, in particular the one measured following the 2005 wet period. This could be explained by an increase of the groundwater head gradient and a change of the flow direction (Bugai et al., 2012a), which could have impacted the spatial distribution of  $^{90}\text{Sr}$  activity into the contaminant plume. The flow-and-transport model also simulates a continuous increasing trend of the  $^{90}\text{Sr}$  activity in groundwater since 1987. However, the model does not consider a possible long-term decrease of  $^{90}\text{Sr}$  mobility in the unsaturated and saturated zones. A progressive decrease of concentrations of major cations (in particular calcium and stable strontium) in groundwater was yet highlighted and could have reduced competition for exchange sites in solid matrix (Bugai et al., 2012b).

## 6. Conclusion

This study shows that inter-annual variability in hydrological processes, especially the recharge rate and the groundwater level, can have a strong influence on the measured activity of high-mobility radionuclides in groundwater downstream of an *in situ* waste disposal. Low-frequency activity measurements are thus complex to interpret since they can sample peaks of activity resulting from relatively wet periods, hiding possible long-term trends induced by climate and land use changes or evolution of geochemical conditions. When considering several decades, the estimation of the cumulative amount of radionuclides released to groundwater could mainly depend on such trends.

The quantification of the sensitivity of the radionuclide activity in groundwater downstream of a waste disposal to each of the transient processes involved thus represents a crucial issue. This requires (i) to establish survey strategies (e.g., sampling frequency, spatial and temporal support of the measurements) which allow to reconstruct the time series of the variables under interest at relevant time scales; and (ii) to conceptualize the main mechanisms that govern radionuclide migration through modelling tools which are consistent with the available knowledge and data. These tasks are complex since they often imply further metrological development and they tackle the scale effect problem.

## Acknowledgments

This study benefited from the Kri-Terres project, supported by the French National Radioactive Waste Management Agency (ANDRA) under the French “Investments for the Future” Program. The authors thank Marc Bourgeois (IRSN) for his helpful relevant advice and assistance on the code MELODIE.

## References

- Ahamdach, N. 2002. The Chernobyl pilot site project: Isolation and microscopic characterization of fuel particles. *Radioprotection*, 37(C1), 1055-60. 10.1051/radiopro/2002124
- Allen, R.G., Pereira, L.S., Raes, D., Smith, M. 1998. Crop evapotranspiration, guidelines for computing crop water requirements FAO Irrigation and drainage paper 56.
- Allen, A., Chapman, D. 2001. Impacts of afforestation on groundwater resources and quality. *Hydrogeol. J.*, 9, 390-400. 10.1007/s100400100148
- AppEARS Team. 2020. Application for Extracting and Exploring Analysis Ready Samples (AppEARS). Ver. 2.54. NASA EOSDIS Land Processes Distributed Active Archive Center (LP DAAC), USGS/Earth Resources Observation and Science (EROS) Center, Sioux Falls, South Dakota, USA. Accessed January 29, 2021. <https://lpdaacsvc.cr.usgs.gov/appears>

- Ardois, C., Szentnect, S. 2005. Capability of the Kd model to predict radionuclides behaviour and transport in unsaturated columns under steady flow conditions. *Radioprotection*, 40, S53-S59. 10.1051/radiopro:2005s1-009
- Balonov, M.I. and Coauthors. 2010. Handbook of Parameter Values for the Prediction of Radionuclide Transfer in Terrestrial and Freshwater Environments. IAEA Technical Report Series No. 472.
- Bugai, D., Dewiere, L., Kashparov, V., Ahamdach., N. 2002. Strontium-90 transport parameters from source term to aquifer in the Chernobyl Pilot Site. *Radioprotection*, 37(C1), 11-16. 10.1051/radiopro/2002024
- Bugai, D., Dewiere, L. 2003. Geostatistical analysis of activity of <sup>137</sup>Cs in Trench no.22 Chernobyl Pilot Site. Technical Report, IRSN/DPRE/SERGD 03-18. 10.13140/RG.2.1.1392.2325
- Bugai, D., Dewiere, L., 2004. Geology structure and hydrogeology conditions of the Chernobyl Pilot Site. Technical report, IRSN/DEI/SARG 04-16. 10.13140/RG.2.1.4992.1048
- Bugai, D., Kashparov, V., Dewiere, L., Khomutinin, Y., Levchuk, S., Yoschenko, V. 2005. Characterization of subsurface geometry and radioactivity distribution in the trench containing Chernobyl clean-up wastes. *Environ. Geol.*, 47, 869-881. 10.1007/s00254-004-1218-6
- Bugai, D., Skalsky, A., Dzhepo, S., Kubko, Y., Kashparov, V., Van Meir, N., Stammose, D., Simonucci, C., Martin-Garin, A. 2012a. Radionuclide migration at experimental polygon at Red Forest waste site in Chernobyl zone. Part 2: Hydrogeological characterization and groundwater transport modeling. *J. Appl. Geochem.*, 27(7), 1359-1374. 10.1016/j.apgeochem.2011.09.028
- Bugai, D., Tkachenko, E., Van Meir, N., Simonucci, C., Martin-Garin, A., Roux, C., Le Gal La Salle, C., Kubko, Y. 2012b. Geochemical influence of waste trench no. 22T at Chernobyl Pilot Site at the aquifer: Long-term trends, governing processes, and implications for radionuclide migration. *J. Appl. Geochem.*, 27(7), 1320-1338. 10.1016/j.apgeochem.2011.09.021
- Burger, A., Lichtscheidl, I. 2019. Strontium in the environment: Review about reactions of plants towards stable and radioactive strontium isotopes. *Sci. Total Environ.*, 653, 1458-1512. 10.1016/j.scitotenv.2018.10.312
- Corcho-Alvarado, J. A., Balsiger, B., Sahli, H., Astner, M., Byrde, F., Röllin, S., Holzer, R., Mosimann, N., Wüthrich, S., Jakob, A., Burger, M. 2016. Long-term behavior of <sup>90</sup>Sr and <sup>137</sup>Cs in the environment: Case studies in Switzerland. *J. Environ. Radioact.*, 160, 54-63. 10.1016/j.jenvrad.2016.04.027
- Dewiere, L., Bugai, D., Grenier, C., Kashparov, V., Ahamdach, N. 2004. Sr-90 migration to the geosphere from a waste burial in the Chernobyl exclusion zone. *J. Environ. Radioact.*, 74, 139-50. 10.1016/j.jenvrad.2004.01.019
- Dzhepo, S., Skalsky, A., Bugai, D., Marchuk, V., Waters, R. 1994. Hydrogeological influences on radionuclide migration from the major radioactive waste burial sites at Chernobyl (A review). International Symposium Sarcophagus Safety'94, Chernobyl. 10.13140/2.1.4138.3684
- Fretwell, B.A., Burgess, W.G., Barker, J.A., Jefferies, N.L. 2005. Redistribution of contaminants by a fluctuating water table in a micro-porous, double-porosity aquifer: field observations and model simulations. *J Contam Hydrol.*, 78(1-2), 27-52. 10.1016/j.jconhyd.2005.02.004
- Garten Jr, C.T. 1999. Modeling the potential role of a forest ecosystem in phytostabilization and phytoextraction of <sup>90</sup>Sr at a contaminated watershed. *J. Environ. Radioact.*, 43(3), 305-323. 10.1016/S0265-931X(98)00061-7

- Gemitzi, A. 2020. Are vegetation dynamics impacted from a nuclear disaster? The case of Chernobyl using remotely sensed NDVI and land cover data. *Land*, 9, 433. 10.3390/land9110433
- Hargreaves, G.H., Allen, R.G. 2003. History and evaluation of Hargreaves evapotranspiration equation. *J. Irrig. Drain. Eng.*, 129, 53-63. 10.1061/(ASCE)0733-9437(2003)129:1(53)
- Healy, R.W., Cook, P.G., 2002. Using groundwater levels to estimate recharge. *Hydrogeol. J.* 10, 91-109. 10.1007/s10040-001-0178-0
- Jackson, C.R., Wang, L., Pachocka, M., Mackay, J., Bloomfield, J. 2016. Reconstruction of multi-decadal groundwater level time-series using a lumped conceptual model. *Hydrol. Process.* 30. 3107-3125. 10.1002/hyp.10850
- Kashparov, V., Ahamdach, N., Dewiere, L. 2004. Trench Source Term Characterization on the Chernobyl Pilot Site. Technical report, IRSN/DEI/SARG 04-14
- Kashparov, V., Yoschenko, V., Levchuk, S., Van Meir, N., Simonucci, C., Martin Garin, A. 2012. Radionuclide migration in the experimental polygon of the Red Forest waste site in the Chernobyl zone - Part 1: Characterization of the waste trench, fuel particle transformation processes in soils, biogenic fluxes and effects on biota. *J. Appl. Geochem.*, 27. 1348-1358. 10.1016/j.apgeochem.2011.11.004
- Kashparov V., Salbu B., Simonucci C., Levchuk S., Reinoso-Maset E., Lind O.C., Maloshtan I., Protsak V., Courbet C., Nguyen H. 2020. Validation of a fuel particle dissolution model with samples from the Red Forest within the Chernobyl exclusion zone. *J Environ Radioact.*, 223-224. 10.1016/j.jenvrad.2020.106387
- Klein Tank, A.M.G., Wijngaard, J.B., Können, G.P., and Coauthors, 2002. Daily dataset of 20th-century surface air temperature and precipitation series for the European Climate Assessment. *Int. J. Climatol.*, 22, 1441-1453. 10.1002/joc.773
- Kuriny, V.D., Ivanov, Y.A., Kashparov, V., Loshchilov, N.A., Protsak, V., Yudin, E.B., Zhurba, M., Parshakov, A.E. 1993. Particle associated Chernobyl fall-out in the local and intermediate zones. *Annals of Nuclear Energy*, 20, 415-420. 10.1016/0306-4549(93)90067-Y
- Le Gal La Salle, C., Aquilina, L., Fourre, E. and Coauthors. 2012. Groundwater residence time downgradient of Trench No. 22 at the Chernobyl Pilot Site: Constraints on hydrogeological aquifer functioning. *J. Appl. Geochem.*, 27, 1304-1319. 10.1016/j.apgeochem.2011.12.006
- Mackay, J.D., Jackson, C.R., Wang, L. 2014. A lumped conceptual model to simulate groundwater level time-series. *Environ. Model. Softw.*, 61, 229-245. 10.1016/j.envsoft.2014.06.003
- Matoshko, A., Bugai, D., Dewière, L., Skalsky, A. 2004. Sedimentological study of the Chernobyl NPP site to schematise radionuclide migration conditions. *Environ. Geol.* 46, 820-830. 10.1007/s00254-004-1067-3
- McCarthy, J., Czerwinski, K., Sanford, W., Jardine, P., Marsh, J.D. 1998. Mobilization of transuranic radionuclides from disposal trenches by natural organic matter. *J. Contam. Hydrol.*, 30, 49-77. 10.1016/S0169-7722(97)00032-6
- Nash, J.E., Sutcliffe, J.V. 1970. River flow forecasting through conceptual models part I - a discussion of principles. *J. Hydrol.*, 10, 282-290. 10.1016/0022-1694(70)90255-6
- Nguyen H.L. 2017. Contribution à la quantification des incertitudes portées par la variabilité spatiale des déchets radioactifs enterrés à Tchernobyl. PhD thesis, MINES ParisTech, PSL Research University.

- Pannecoucke, L., Le Coz, M., Houzé, C., Saintenoy, A., Cazala, C., de Fouquet, C. 2019. Impact of spatial variability in hydraulic parameters on plume migration within unsaturated surficial formations. *J. Hydrology.*, 574, 160-168. 10.1016/j.jhydrol.2019.04.016
- Roebroek, C.T.J., Melsen, L.A., Hoek van Dijke, A.J., Fan, Y., Teuling, A. J. 2020. Global distribution of hydrologic controls on forest growth. *Hydrol. Earth Syst. Sci.*, 24, 4625-4639, doi.org/10.5194/hess-24-4625-2020
- Saintenoy, A., Courbet, C., Nguyen, L., Léger, E., & Bugai, D. 2017. Results from two GPR surveys (2002 and 2015) in the Chernobyl exclusion zone. In 2017 9th International Workshop on Advanced Ground Penetrating Radar (IWAGPR) (pp. 1-6), IEEE. 10.1109/IWAGPR.2017.7996094
- Saprykin, V.Y., Bugai, D., Skalskyi, O.S., Kubko, Y., 2015. Method for groundwater recharge and specific yield coefficient estimation for sandy soils using water table fluctuations analysis. *Geol. J.*, 1, 88-98.
- Steeffel, C., Carroll, S., Zhao, P., Roberts, S. 2004. Cesium migration in Hanford sediment: A multisite cation exchange model based on laboratory transport experiments. *J. Contam. Hydrol.*, 67, 219-246. 10.1016/S0169-7722(03)00033-0
- Thiery, D. 1988. Forecast of changes in piezometric levels by a lumped hydrological model. *J. Hydrol.*, 97, 129-148. 10.1016/0022-1694(88)90070-4
- Thiery, D. 2015. Validation du code de calcul GARDÉNIA par modélisations physiques comparatives. BRGM Report RP-64500-FR.
- Thiry, Y., Colle, C., Yoschenko, V., Levchuk, S., Hees, M., Hurtevent, P., Kashparov, V. 2009. Impact of Scots pine (*Pinus sylvestris* L.) plantings on long term Cs-137 and Sr-90 recycling from a waste burial site in the Chernobyl Red Forest. *J. Environ. Radioact.*, 100, 1062-1068. 10.1016/j.jenvrad.2009.05.003
- Van Meir, N., Bugai, D., Kashparov, V. 2009. The Experimental Platform in Chernobyl: An International Research Polygon in the Exclusion Zone for soil and groundwater contamination. In *Radioactive Particles in the Environment*, 197-208. 10.1007/978-90-481-2949-2\_13
- Van Meir, N., Gaudet, J.P., Phrommavanh, V., Laurent, J.P., Bugai, D., Biron R. 2012. Flow in the unsaturated zone around a shallow subsurface radioactive waste trench: Interpretation of an infiltration–drainage test at the Chernobyl Pilot Site. *J. Appl. Geochem.*, 27(7), 1297-1303. 10.1016/j.apgeochem.2011.08.009
- Xu, C. 2003. WASMOD - The water and snow balance modeling system. In: *Mathematical Models of Small Watershed Hydrology and Applications*, *J. Environ. Qual.*, 32. 10.2134/jeq2003.374a
- Zhuang, J., McCarthy, J., Tyner, J., Perfect, E., Flury, M. 2007. *In situ* colloid mobilization in Hanford sediments under unsaturated transient flow conditions: effect of irrigation pattern. *Environ. Sci. Technol.*, 41, 3199-3204. 10.1021/es062757h

## Figures

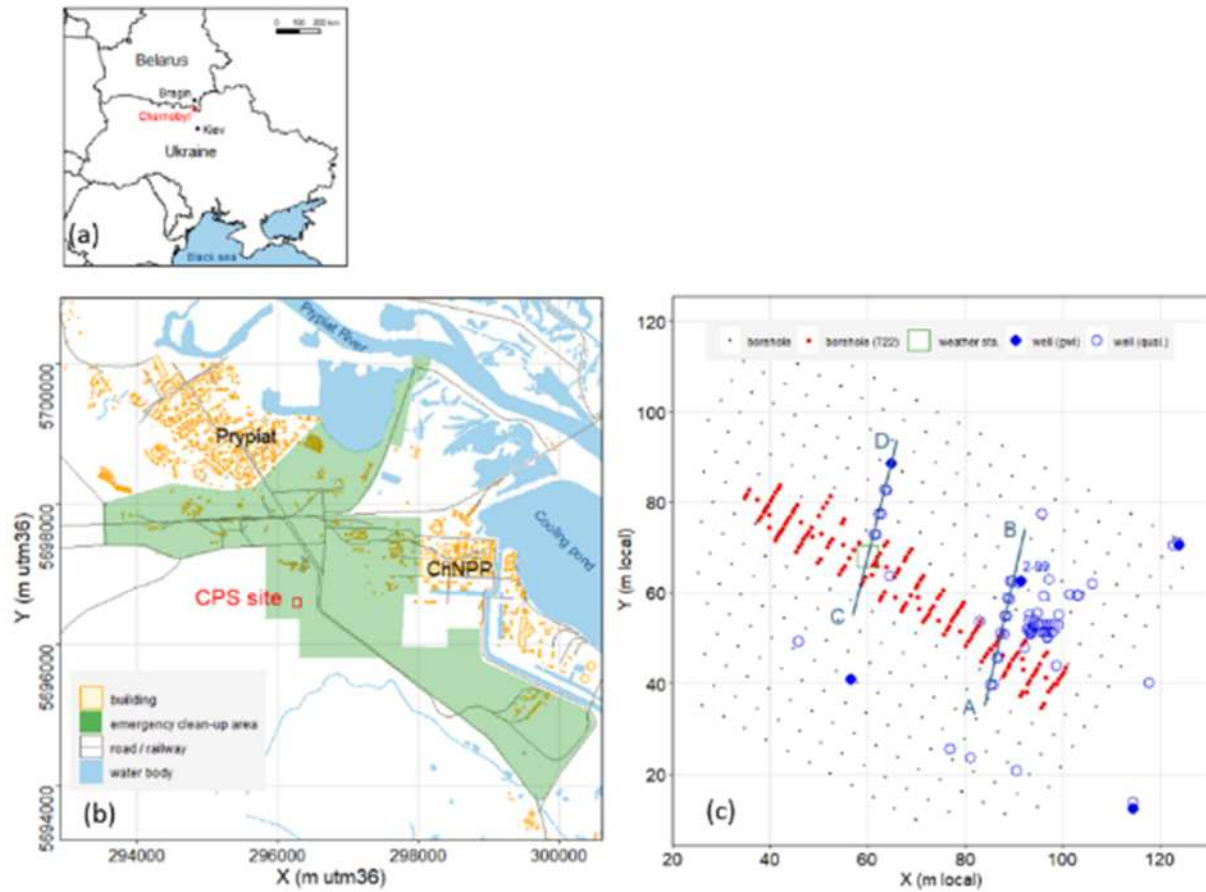


Figure 1. Location of the Chernobyl Pilot Site (CPS) in Ukraine (a) and in the Chernobyl emergency clean-up area (from Bugai et al., 2005) (b); and main surveying equipment installed in the CPS (c). The lines A-B and C-D correspond to the 2-D vertical cross-sections considered for the analysis of  $^{90}\text{Sr}$  activities.

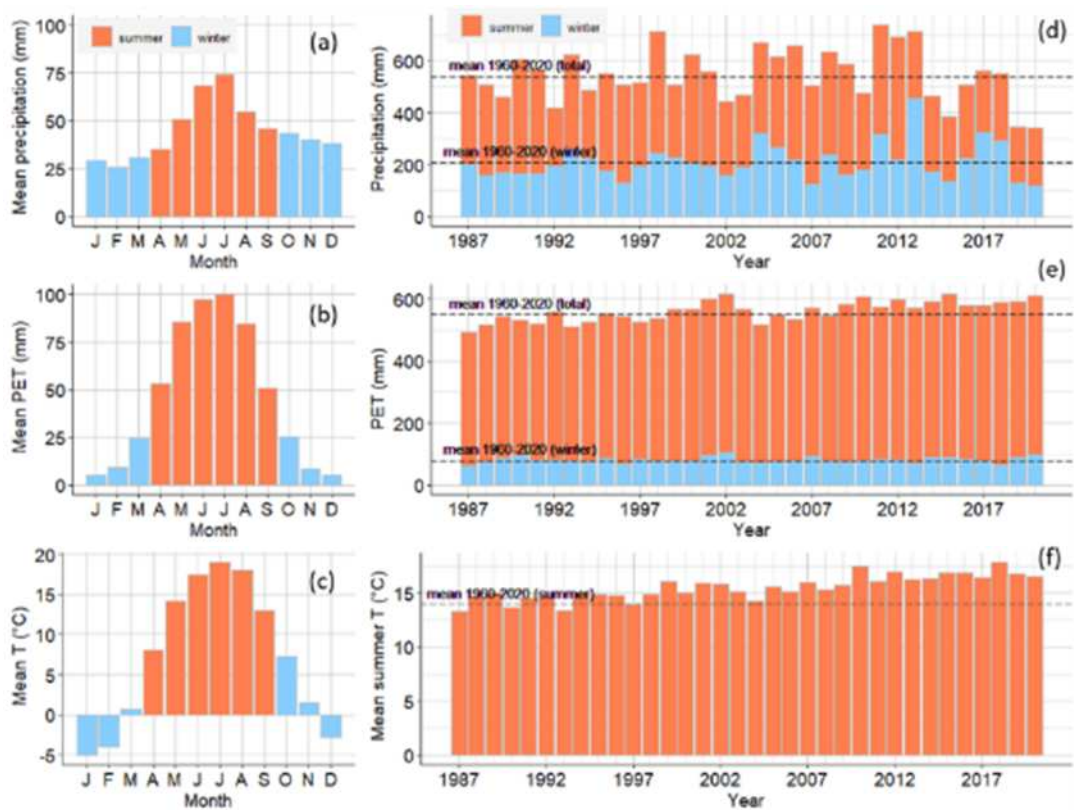


Figure 2. Monthly precipitation (a), potential evapotranspiration (PET) (b) and air temperature (c) computed for the CPS from 1960 to 2020 based on reconstructed time-series. Yearly cumulative precipitation (d) and PET (e), and average summer temperature (f) from 1997 to 2020.

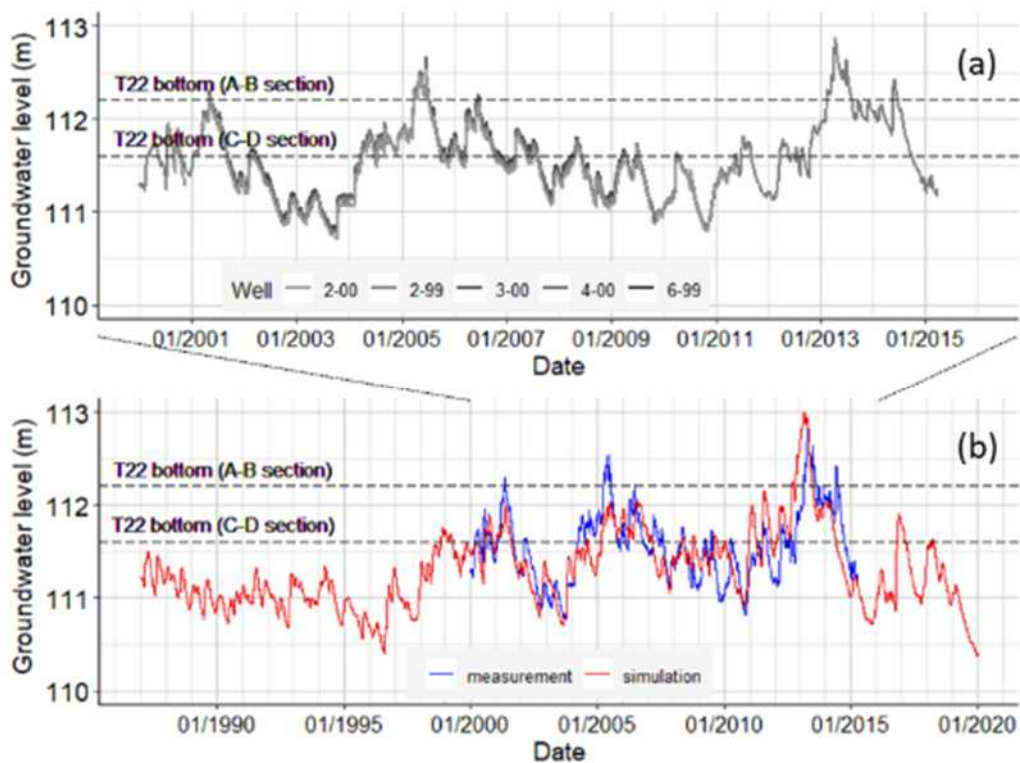


Figure 3. Water level measured in monitored wells from 2000 to 2015 (a); and 1987-2020 time-series reconstructed through the groundwater fluctuation model (Annex 1) (b).

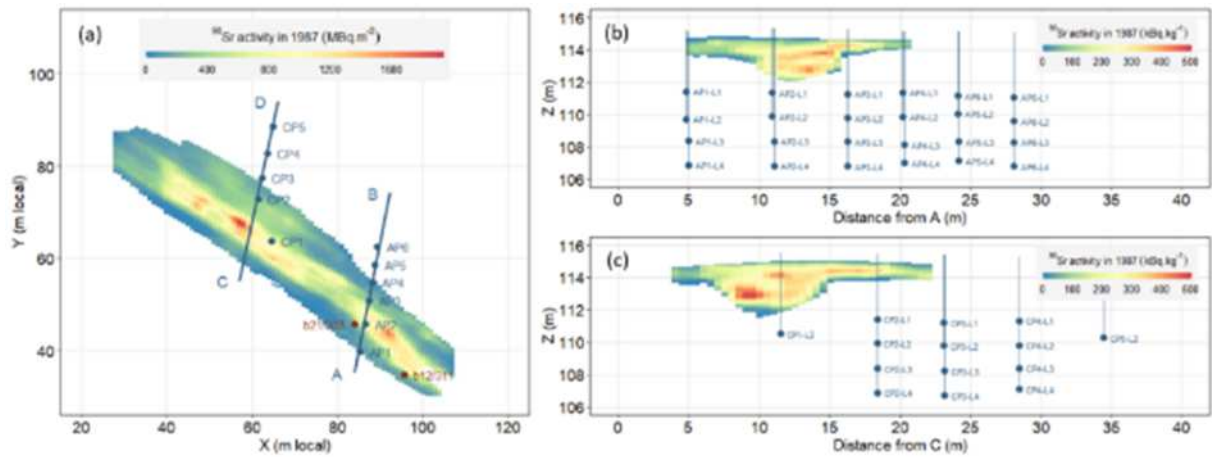


Figure 4. Views of the 3-D model of  $^{90}\text{Sr}$  inventory in 1987 (computed from the mean  $^{137}\text{Cs}$  inventory estimated by Nguyen, 2017) and location of the wells monitored for groundwater activity survey: horizontal view with cumulative  $^{90}\text{Sr}$  activity in depth (a); and views of the A-B (b) and C-D (c) cross-sections.

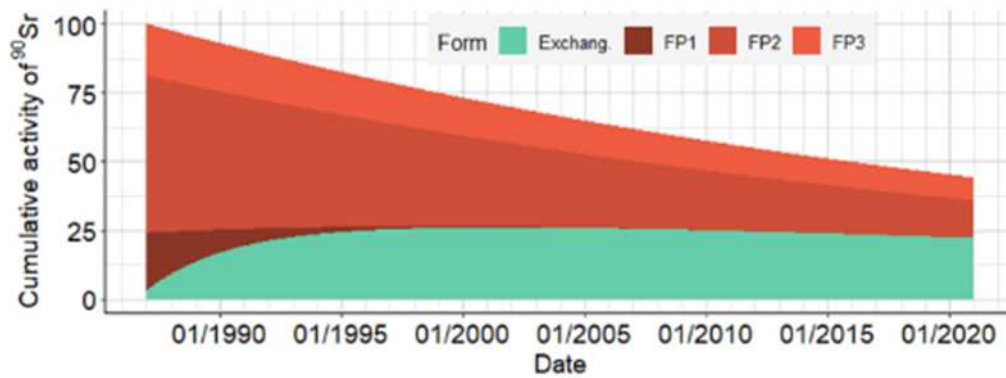


Figure 5. Estimated proportions of each form of the  $^{90}\text{Sr}$  since 1987 estimated based on the fuel particle dissolution model established for waste material from the trench T22 (Annex 2).

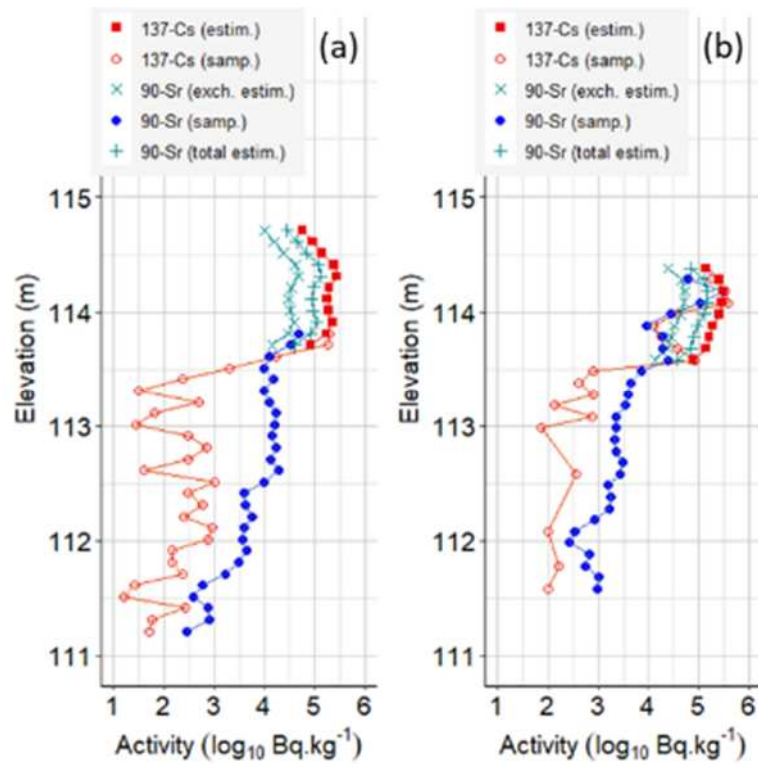


Figure 6. Activity of total  $^{90}\text{Sr}$  and  $^{137}\text{Cs}$  in 2000 measured in samples and activity of  $^{137}\text{Cs}$  and  $^{90}\text{Sr}$  deduced from the 3-D model of  $^{137}\text{Cs}$  inventory (Nguyen, 2017) and the fuel particle dissolution model (Annex 2) in boreholes (a) b21/303; and (b) b12/311.

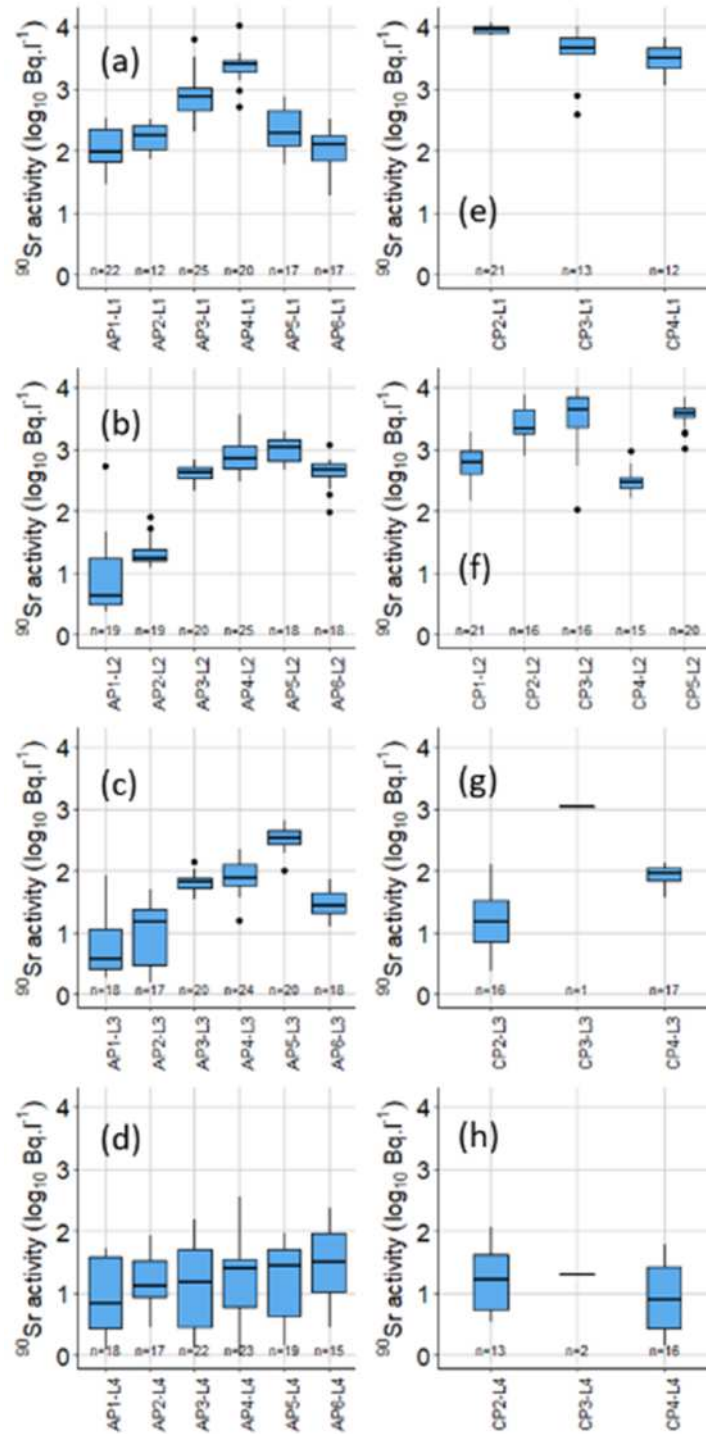


Figure 7. Box-plots of the  $^{90}\text{Sr}$  activities measured in groundwater sampled from 2000 to 2015 in layers L1 to L4 of piezometers (a-d) AP1 to AP6 and (e-h) CP1 to CP5. These plots show the spatial distribution of the  $^{90}\text{Sr}$  activity in the aquifer underlying the trench T22.

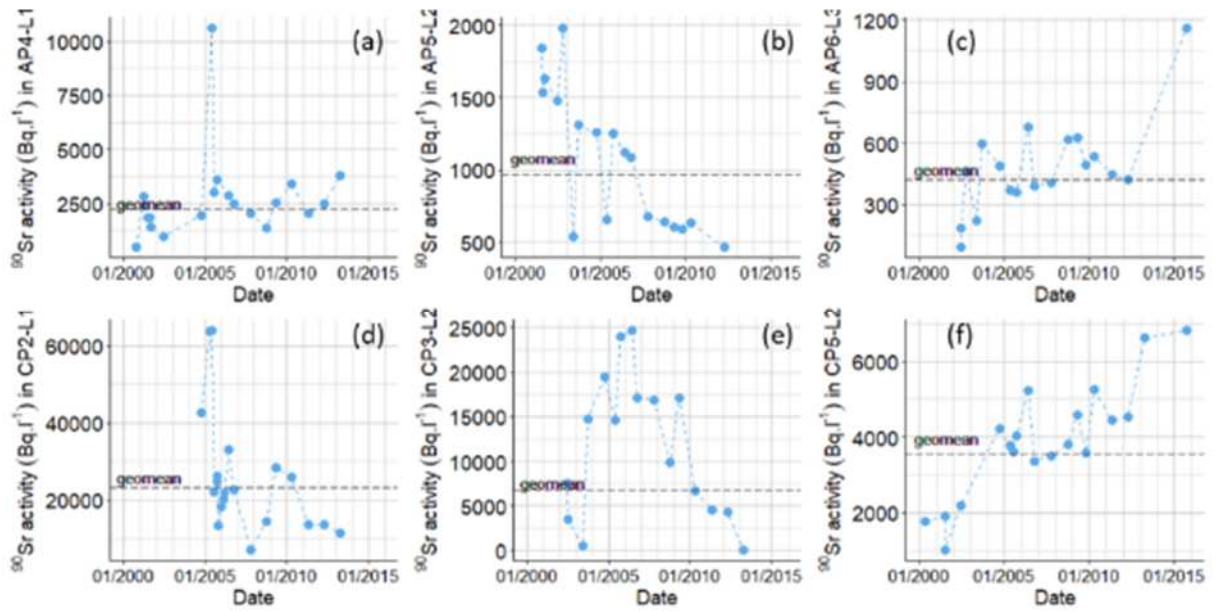


Figure 8. Activity in  $^{90}\text{Sr}$  measured in groundwater sampled from 2000 to 2015 in the  $^{90}\text{Sr}$  plume downstream from the trench T22 in piezometers AP4-L1 (a), AP5-L2 (b) and AP6-L2 (c) and CP2-L1 (d), CP3-L2 (e) and CP5-L2 (f).

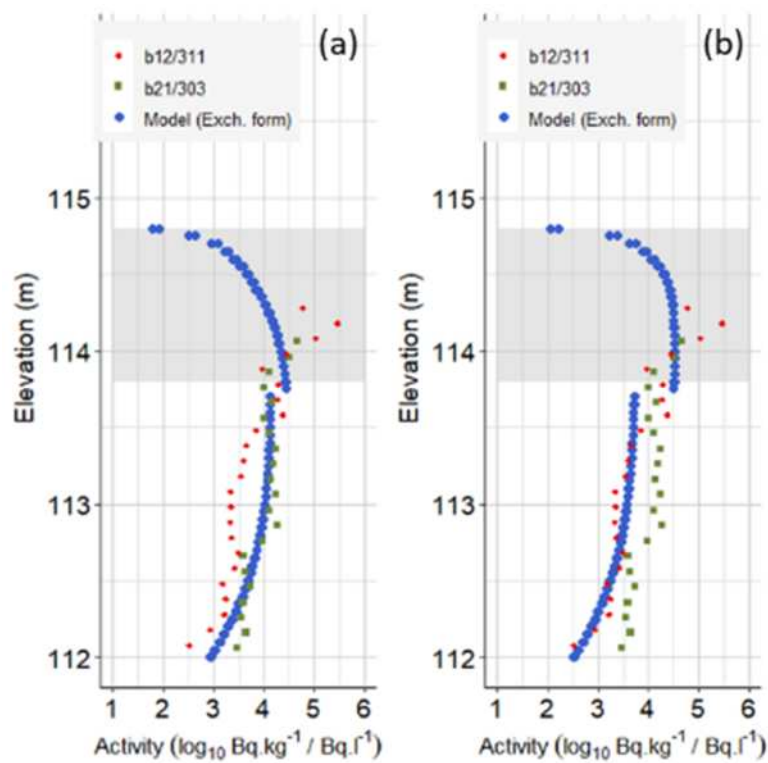


Figure 9. Activity of total  $^{90}\text{Sr}$  and in 2000 measured in samples and of ion-exchangeable  $^{90}\text{Sr}$  simulated with the flow-and-transport model in boreholes b21/303 and b12/311 with (a)  $R=10$ ; and  $R=25$  (b).

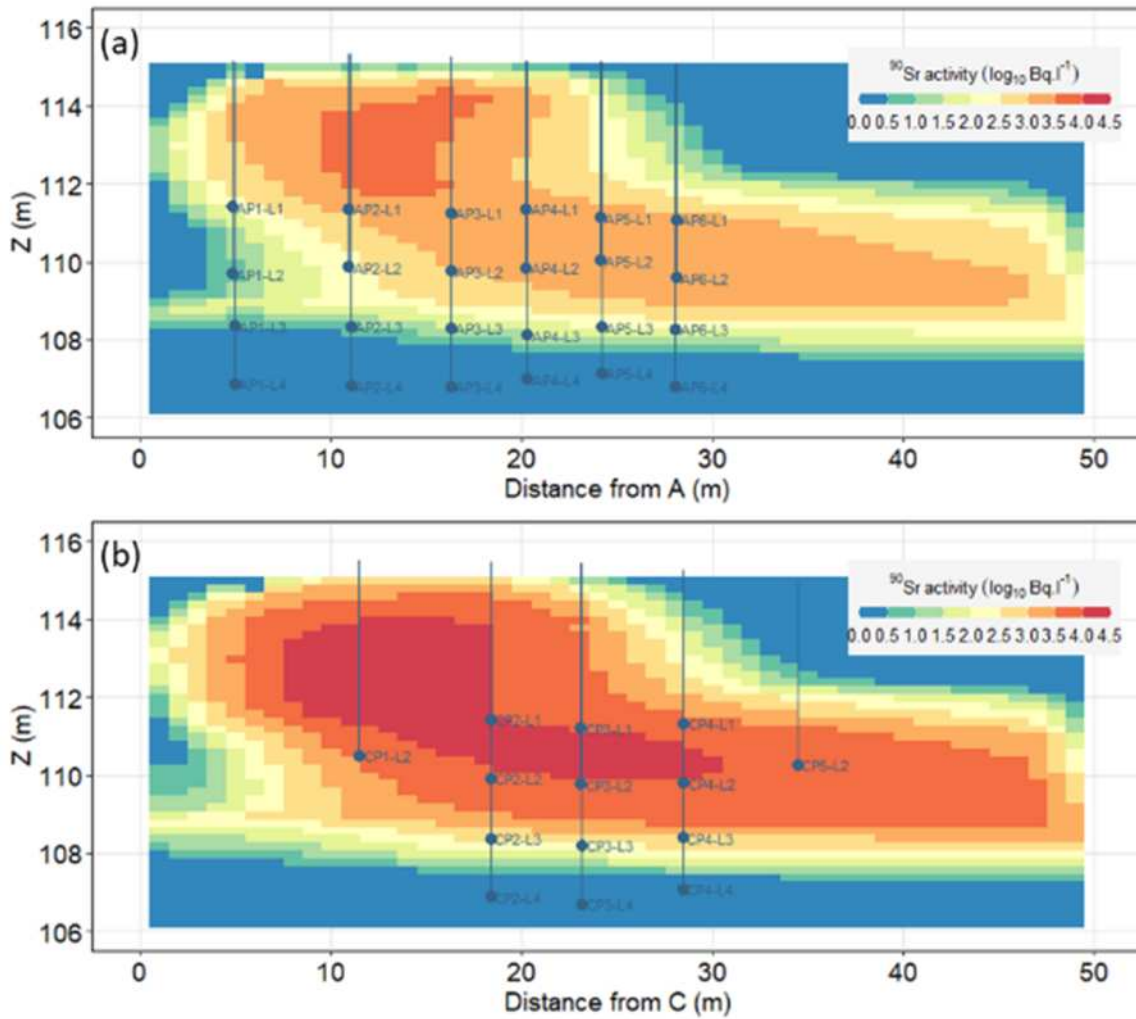


Figure 10. Activity of ion-exchangeable  $^{90}\text{Sr}$  simulated in 2015 with the flow-and-transport model along the cross-sections (a) A-B ( $R=50$ ); and (b) C-D ( $R=13$ ).

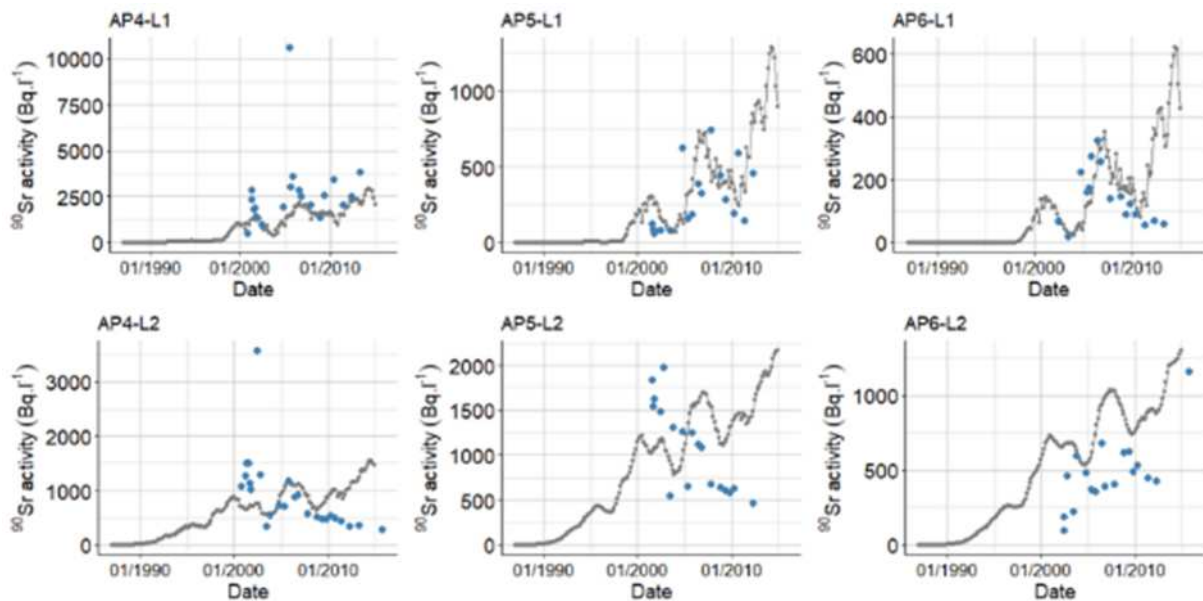


Figure 11. Activity of ion-exchangeable  $^{90}\text{Sr}$  measured (circles) and simulated (line) from 1987 to 2015 with the flow-and-transport model in the piezometers located along the cross-sections A-B ( $R=50$ ).

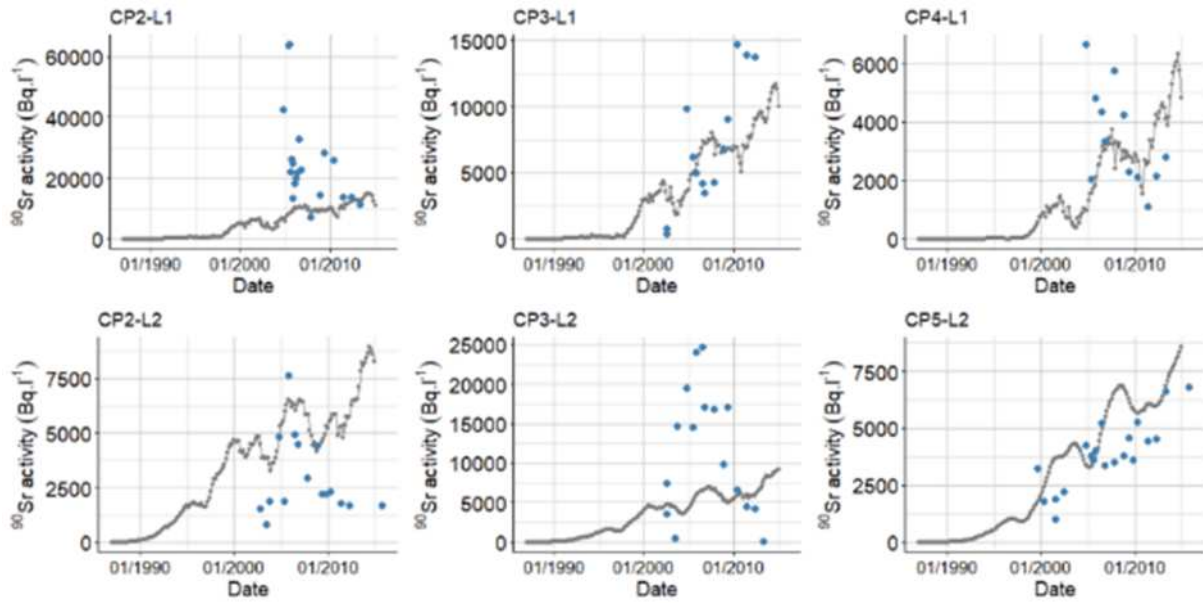


Figure 12. Activity of ion-exchangeable  $^{90}\text{Sr}$  measured (circles) and simulated (line) from 1987 to 2015 with the flow-and-transport model in the piezometers located along the cross-sections C-D ( $R=13$ ).

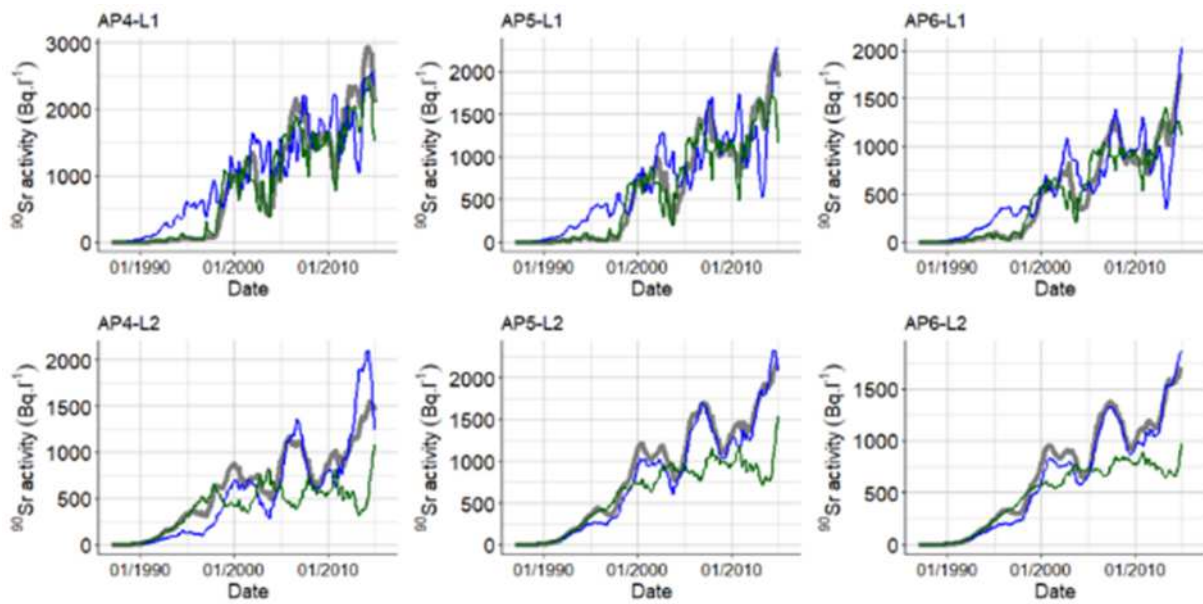


Figure 13. Activity of ion-exchangeable  $^{90}\text{Sr}$  simulated from 1987 to 2015 with the flow-and-transport model in the piezometers located along the cross-sections A-B by considering a temporal variability of both the recharge rate and the groundwater level (grey line); the recharge rate only (green line); the groundwater level only (blue line).

### Tables

Table 1. Comparison of daily precipitation released by the European Climate Assessment & Dataset (ECA&D) project at four stations with CPS data. Wet days corresponds to days with precipitation > 0.5 mm.

Station name	Location (km from CPS)	Comparison period (days)	Cumulative precipitation (% CPS)	Number of wet days (% CPS)	Common wet / not-wet days (%)
Kiev	100 km (S)	2973	88	96	75

Vasilevici	100 km (N)	2971	85	89	76
Mozyr	90 km (N-NW)	2973	83	58	77
Bragin	50 km (N)	2973	97	99	80

Table 2. Pearson correlation coefficients computed from daily time-series of groundwater fluctuation model (input: precipitation and potential evaporation, PET; output: percolation and actual evapotranspiration, AET) for winter (upper triangle) and summer (lower triangle) periods.

	Precipitation	Percolation	AET	PET
Precipitation		0.99	0.01	-0.24
Percolation	0.86		-0.04	-0.27
AET	0.83	0.47		0.63
PET	-0.35	-0.23	-0.40	

Table 3. Parameters of the flow-and-transport model.

			Waste (T22)	Eolian sand	Alluvial sand
Flow parameters	Retention / relative K curves (Mualem-van Genuchten model)	$\alpha$	3.5 m <sup>-1</sup>		-
		$n$	1.5		-
		$\vartheta_{res}$	0.05		-
		$\vartheta_{sat}$	0.38	0.30	-
	K	$K_x$	5 m.d <sup>-1</sup>		1 m.d <sup>-1</sup>
		$K_z$	0.5 m.d <sup>-1</sup>	5 m.d <sup>-1</sup>	0.01 m.d <sup>-1</sup>
Transport parameters	$d$		10 <sup>-5</sup> m <sup>2</sup> .d <sup>-1</sup>		
	D	$D_x$	0.05 m		
		$D_z$	0.005 m		
	$\omega$		0.38	0.30	0.4
	$\omega'$	<i>unsaturated</i>	0.38	0.30	-
		<i>saturated</i>	0.38	0.1	0.1
	R		10-50	3	12

Table 4. Cumulative annual precipitation and percolation estimated through the groundwater fluctuation model (this study) and WTF method (Saprykin et al., 2015) from 2000 to 2012.

Year	Precipitation (mm)	Percolation - GW fluctuation model (mm)	Percolation - WTF method (mm)
2000	596	274	329
2001	554	179	257
2002	495	171	210
2003	513	198	242
2004	618	271	417
2005	652	351	326
2006	575	208	234
2007	561	157	259
2008	578	240	298
2009	656	264	277
2010	576	216	300
2011	585	258	245
2012	877	462	439

Table A1-1. Calibrated parameters (for the 2000-2015 period) of the groundwater fluctuation model.

$a_1$ - upper threshold temperature (°C)	4
$a_2$ - lower threshold temperature (°C)	-4
$SRC$ - soil reservoir capacity (mm)	20
$THG$ - UZ reservoir residence time (days)	30
$\omega$ - aquifer material effective porosity (%)	5
$TG1$ - SZ1 reservoir residence time (days)	90
$TG2$ - SZ1 reservoir residence time (days)	900

Table A2-2. Dissolution model parameters for trench T22 conditions (from Kashparov et al., 2012): dissolution constants and initial fractions for each FP type.

	FP1	FP2	FP3
$\alpha_i$ (y-1)	0.28 ( $\pm$ 0.05)	0.018 ( $\pm$ 0.001)	$\approx$ 0
$E_i$ (%)	21 ( $\pm$ 15)	57 ( $\pm$ 15)	19 ( $\pm$ 10)

## Annex 1 - A groundwater level fluctuation model for reconstructing water table time-series

### A1.1. Conceptual lumped models of groundwater level fluctuation

Conceptual lumped parameter modelling can be used to simulate water table level time-series by neglecting some of the complexities incorporated in physically-based model, but maintaining some fundamental physical principles from our conceptual understanding of the groundwater system (Mackay et al., 2014). These types of models consists of generic components that corresponds to water cycle processes from a functional perspective (Jackson et al., 2016).

In this study, a model structure is build based on modules of the model GARDENIA (Thiery, 1988, Thiery, 2015), i.e., interconnected reservoirs representing soil, unsaturated and saturated zones. An additional reservoir is implemented for simulating snowpack (Xu, 2003). Saturated zone is conceptualized through two units, an upper unit responsible for high-frequency (intra-annual) variations in water table level; and a lower unit responsible for low-frequency (inter-annual) variations. Runoff is neglected since topography of the area is flat and infiltration capacity is relatively high.

### A1.2. Model structure

Model input are precipitation, potential evapotranspiration (PET) and average air temperature, at a daily time step.

Snowpack is fed by snowfall and supplies soil reservoir through snowmelt. Both partitioning of precipitation into rainfall and snowfall and snowmelt are calculated as a function of average air temperature:

$$Sn_i = \begin{cases} P_i \times \left[ 1 - e^{(-1) \times \left( \frac{T_i - a_1}{a_1 - a_2} \right)^2} \right], & T_i < a_1 \\ 0, & T_i \geq a_1 \end{cases} \quad [A1-1]$$

$$SPout_i = \begin{cases} SP_i \times \left[ 1 - e^{(-1) \times \left( \frac{T_i - a_1}{a_1 - a_2} \right)^2} \right], & T_i \geq a_2 \\ 0, & T_i < a_2 \end{cases} \quad [A1-2]$$

where  $Sn_i$  and  $SPout_i$  are snowfall and snowmelt for day  $i$  (mm);  $T_i$  is daily air temperature (°C);  $P_i$  is daily precipitation (mm);  $SP_i$  is snowpack height (mm); and  $a_1$  and  $a_2$  are threshold temperature parameters (°C).

Soil reservoir is fed by rainfall and snowmelt. Evapotranspiration is withdrawn and water excess supplies unsaturated zone reservoir:

$$AET_i = \begin{cases} PET_i, & (SR_i + R_i + SPout_i) \geq PET_i \\ SR_i + R_i + SPout_i, & (SR_i + R_i + SPout_i) < PET_i \end{cases} \quad \text{with } R_i = P_i - Sn_i \quad [A1-3]$$

$$SRout_i = \begin{cases} (SR_i + R_i + SPout_i) - SRC, & (SR_i + R_i + SPout_i) > SRC \\ 0, & (SR_i + R_i + SPout_i) \leq SRC \end{cases} \quad [A1-4]$$

where  $AET_i$  and  $SRout_i$  are actual evapotranspiration and soil water excess for day  $i$  (mm);  $PET_i$  is daily potential evapotranspiration (mm);  $SR_i$  is soil reservoir level (mm);  $R_i$  is rainfall (mm); and  $SRC$  is soil reservoir capacity parameter (mm).

Unsaturated zone reservoir is fed by water excess from soil reservoir and percolation supplies saturated zone:

$$UZRout_i = \frac{UZ_i}{THG} \quad [A1-5]$$

where  $UZRout_i$  is percolation for day  $i$  (mm);  $UZ_i$  is unsaturated zone reservoir level (mm); and  $THG$  is a time parameter (day).

Hydraulic head fluctuation in upper unit of saturated zone is governed by percolation from unsaturated zone and leakage to lower unit:

$$\partial HSZ1_i = \left( UZRout_i \times \frac{\omega}{1000} \right) - \frac{HSZ1_{i-1}}{TG1} \quad [A1-6]$$

where  $\partial HSZ1_i$  is variation in hydraulic head in upper unit of saturated zone for day  $i$  (m);  $\omega$  is aquifer material porosity (-);  $HSZ1_{i-1}$  is hydraulic head for day  $i - 1$  (m); and  $TG1$  is a time parameter (day).

Hydraulic head fluctuation in lower unit of saturated zone is governed by leakage from upper layer and aquifer outflow:

$$\partial HSZ2_i = \frac{HSZ1_{i-1}}{TG1} - \frac{HSZ2_{i-1}}{TG2} \quad [A1-7]$$

where  $\partial HSZ2_i$  is variation in hydraulic head of lower unit of saturated zone for day  $i$  (m);  $HSZ2_i$  is hydraulic head for day  $i - 1$  (m); and  $TG2$  is a time parameter (day).

### A1.3. Model parameters

Model parameters are adjusted based on the Nash-Sutcliffe efficiency criteria (Nash and Sutcliffe, 1970), so as to simulated variations in groundwater level fit observed time-series at the well 2-99 for the whole 2000-2015 period (Table A1-1).

## Annex 2 - Initial inventory of $^{90}\text{Sr}$ and release in ion-exchangeable form

### A2.1. From $^{137}\text{Cs}$ in 2000 to $^{90}\text{Sr}$ in 1987

Direct correlation between activities of  $^{90}\text{Sr}$  and  $^{137}\text{Cs}$  measured in samples collected within the trench T22 is relatively poor since  $^{90}\text{Sr}$  has been redistributed inside and outside the trench due to hydrogeologic migration processes that occurred between 1987 and 1999-2000 (Bugai et al., 2002). By contrast,  $^{154}\text{Eu}$  is a relatively immobile radionuclide and a good correlation with  $^{137}\text{Cs}$  was highlighted (Bugai et al., 2002):

$$[^{137}\text{Cs}]_{2000} = 145 \times [^{154}\text{Eu}]_{2000} \quad [A2-1]$$

where  $[^{137}\text{Cs}]_{2000}$  and  $[^{154}\text{Eu}]_{2000}$  are activities in  $^{137}\text{Cs}$  and  $^{154}\text{Eu}$  ( $\text{Bq}\cdot\text{m}^{-3}$ ) in 2000.

In addition,  $^{154}\text{Eu}$  was associated mainly with fuel matrix and a good correlation exists between  $^{90}\text{Sr}$  and  $^{154}\text{Eu}$  activities in Chernobyl reactor fuel particles. An empirical radionuclide activity ratio was computed based on analysis of fuel and condensed particle components of the Chernobyl fallout (Kuriny et al., 1993):

$$[^{90}\text{Sr}]_{1986} = \frac{100}{3} \times [^{154}\text{Eu}]_{1986} \quad [\text{A2-2}]$$

where  $[^{90}\text{Sr}]_{1986}$  and  $[^{154}\text{Eu}]_{1986}$  are activities in  $^{90}\text{Sr}$  and  $^{154}\text{Eu}$  ( $\text{Bq}\cdot\text{m}^{-3}$ ) in 1986.

Equations A2-1 and A2-2 and radioactive decay of  $^{157}\text{Eu}$  (half-life of 8.6 years) are used for converting the simulated activities in  $^{137}\text{Cs}$  to the initial (1987) activities in  $^{90}\text{Sr}$ .

## A2.2. Fuel particle dissolution model

The radionuclides in the Chernobyl fallout were associated with micron-sized particles of the dispersed nuclear fuel. Observations in the post-accident phase showed that these fuel particles (FP) are subject to gradual dissolution under natural conditions that results in releases of radionuclides into the surrounding environment (Kashparov et al., 2004, 2012).

The  $^{90}\text{Sr}$  is considered to be associated to three main types of FP (Ahamdach, 2002): (i) oxidized FP in a  $\text{UO}_{2+x}$  matrix (FP1); (ii) non-oxidized FP in a  $\text{UO}_2$  matrix (FP2); and (iii) extra-stable FP in a  $\text{ZrU}_y\text{O}_x$  matrix (FP3). According to this classification and based on several studies focusing on the FP dissolution, the following model was proposed to describe the release of  $^{90}\text{Sr}$  in ion-exchangeable form (Kashparov et al., 2012):

$$F(t) = [^{90}\text{Sr}]_0 \sum_{i=1}^3 E_i \alpha_i e^{-(\lambda + \alpha_i)t} \quad [\text{A2-3}]$$

where  $F(t)$  is the integral flux of  $^{90}\text{Sr}$  in ion-exchangeable form released from FP into a unit volume of waste ( $\text{Bq}\cdot\text{m}^{-3}\cdot\text{day}^{-1}$ ) at time  $t$  (day);  $[^{90}\text{Sr}]_0$  is the integral activity in  $^{90}\text{Sr}$  into a unit volume of waste at time  $t_0$  ( $\text{Bq}\cdot\text{m}^{-3}$ );  $E_i$  is the  $^{90}\text{Sr}$  activity fraction associated with the FP of type  $i$  at time  $t_0$ ;  $\alpha_i$  is an empirical constant of dissolution rate for the FP of type  $i$  ( $\text{day}^{-1}$ ); and  $\lambda$  is the  $^{90}\text{Sr}$  radioactive decay rate ( $\text{day}^{-1}$ ).

The kinematic dissolution constants ( $\alpha_i$ ) and the initial distribution for the different FP types ( $E_i$ ) were deduced from laboratory experiments on waste material from the trench T22 (e.g., Kashparov et al., 2004), and then supported with experimental results (Kashparov et al., 2020) (Table A2-1).